Journal Title
XX(X):1–13
©The Author(s) 2021
Reprints and permission:
sagepub.co.uk/journalsPermissions.nav
DOI: 10.1177/ToBeAssigned
www.sagepub.com/
SAGE

Development and performance evaluation of an electromagnetic transducer with a tuned variable inerter

Minoru Takino[1] and Takehiko Asai[2]

Abstract

This paper proposes a novel vibration energy harvesting device employing a tuned variable inerter. The inerter is a device that can produce an amplified inertial mass effect by ball screw or rack and pinion mechanisms. Originally, the inerter was developed for suspensions in automobiles, and various kinds of inerter technologies have been widely studied not only in structural control but also in energy harvesting so far. As an example of such devices, the tuned inertial mass electromagnetic transducer (TIMET) has been proposed and its effectiveness as an energy harvesting device has been shown already. However, at the same time, previous studies suggested that further performance improvement is possible if the inerter is variable according to changes in disturbance conditions. Thus, in this research, a prototype which can change the value of inerter is designed, and a system to change the inerter based on the dominant frequency detected online by the fast Fourier transform (FFT) of the measured data is developed. Then, it is shown through experimental studies that the proposed device can improve the energy harvesting performance compared to the existing TIMET for disturbances with varying dominant frequencies.

Keywords

Energy harvesting, Electromagnetic transducer, Tuned inerter, Variable inerter, Structural dynamics

Introduction

In response to the growing social interest in renewable energy, vibration energy harvesting technologies have been attracting a lot of attention lately. In particular, to harvest W- to kW-scale power from vibrating structures characterized by frequencies below 10 Hz, an electromagnetic transducer (ET) has been considered to be a promising device (Zuo and Tang 2013; Wei and Jing 2017; Siang et al. 2018). In this device, translational motion is converted to rotational behavior through a ball screw to rotate the motor, and part of the vibration energy of the structure to which the ETs are attached can be absorbed as electrical energy. Additionally, because motors can be used not only as generators but also as actuators, the ETs can be employed as self-powered control devices for vibration suppression of structures, in which the generated energy is reinjected to control the vibrating structure (Nakano et al. 2003; Scruggs and Iwan 2003; Jamshidi et al. 2017; Asai and Scruggs 2016). Some researchers have devoted considerable efforts to improve the performance of the ET so far, however, most of the studies have been focused on developing algorithms to control the input current to the motor and the effect is relatively limited (Cassidy et al. 2011b; Cassidy and Scruggs 2013; Caruso et al. 2018; Monaco et al. 2013; Shen et al. 2019).

On the other hand, to increase the energy absorption capability of the traditional ET by utilizing a simple mechanical system, devices employing an *inerter* mechanism have been introduced. The inerter, which can produce a force proportional to the relative acceleration across its two terminals, was originally introduced by Smith (2002) for vibration suppression of automobiles. And the proportional constant between the inerter and the relative acceleration is called *inertance*, which has the same physical unit as mass. Moreover, large inertance values can be easily realized through a ball screw or a rack-and pinion from relatively small actual masses. Nowadays, this technology is actively applied to civil structures subjected to external loadings such as earthquakes and strong winds for the purpose of vibration suppression. This inerter technology has developed rapidly in this field and many devices with various configurations, including combinations with spring elements, have been proposed so far (Ikago et al. 2012; Marian and Giaralis 2014; Lazar et al. 2014; Ma et al. 2021; Wagg 2021). Especially, in more recent years, to achieve further improvement in structural control performance, several mechanisms such as continuously variable transmission (CVT) (Lazarek et al. 2019) and ball screw with a variable thread lead (Faraj et al. 2019) to make the inerter variable have been proposed.

In addition to the purpose of structural control, various kinds of devices employing the inerter for vibratory energy harvesting have been introduced so far (Gonzalez-Buelga et al. 2015; Asai et al. 2017; Marian and Giaralis 2017; Zhu et al. 2019). Among the energy harvesting devices employing the inerter technology, the second author of this paper has proposed a tuned inertial

[1]Graduate School of Science and Technology, University of Tsukuba, Japan
[2]Faculty of Engineering, Information and Systems, University of Tsukuba, Japan

Corresponding author:
Takehiko Asai, University of Tsukuba, 1-1-1 Tennodai, Tsukuba, Ibaraki 305-8573, Japan
Email: asai@kz.tsukuba.ac.jp

mass electromagnetic transducer (TIMET) (Asai et al. 2017; Sugiura et al. 2020). The TIMET consists of a motor for energy generation, a rotational mass attached to a ball screw for the inerter effect, and a tuning spring. Then, the stiffness of the tuning spring is determined appropriately so that the rotational mass is tuned to the dominant frequency of the vibrating structure. The rotational mass is connected to the motor through the ball screw, so the number of revolutions of the motor can be increased when the rotational mass resonates with the external disturbance, and the the power generation efficiency can be improved. The effectiveness of the TIMET has been shown already through numerical simulation studies (Asai et al. 2017) and experimental studies employing a hardware-in-the-loop (HIL) strategy (Asai et al. 2021) by the authors.

However, because the TIMET takes advantage of the resonance effect, the frequency range in which the TIMET works effectively is limited. Thus, to overcome this weakness, this article proposes a variable inerter mechanism and aims to verify the effectiveness as a energy harvester through excitation testing using a prototype of the proposed device. As explained above, the resonance frequency of the TIMET is determined by the stiffness of the tuning spring and the inertance. Typically, it is difficult, though not impossible, to make the stiffness of the spring variable with a simple mechanism. While, the inerter is produced by rotating some weights utilizing the ball screw. Considering the fact that the inertance highly depends on the radius of rotation of the weights, it is obvious that the resonance frequency of the TIMET can be adjusted by changing the radius of rotation. Therefore, in this research, the authors modify the device developed in the author's previous works (Sugiura et al. 2020; Asai et al. 2021) and design a prototype which can change the inertance value, develop a system to control the inertance based on the dominant frequency calculated by the measured vibration data online. Then, the power generation performance when the inerter variable mechanism is combined with the motor current controller is evaluated through excitation testing. This article is organized as follows. First, the mechanism of the proposed device is illustrated, and the designed prototype of the proposed device is introduced. Then, the problem considered in this paper is formulated and the control algorithms for the variable inerter and the motor are overviewed. Subsequently, the experimental setup and results are presented. Finally, conclusions obtained from this study follow.

Mechanism

First of all, the mechanism of the TIMET is introduced here after reviewing that of the typical ET briefly.

Electromagnetic transducer

Fig. 1 (a) depicts the typical ET schematically. As illustrated, a motor is interfaced with a ball screw and mechanical energy of translational motion is converted to electrical energy by rotating the motor. This device can be modeled simply as shown in Fig. 1 (b), in which m_i is the inertance attributable to the motor and the ball screw, c_m is the inherent unavoidable mechanical damping caused in the device, and c_e is the electromechanical coupling which is determined by the back electromotive force (EMF) constant of the motor K_e and the lead of the ball screw l and defined as (Cassidy et al. 2011a; Sugiura et al. 2020; Asai et al. 2021)

$$c_e = \frac{\sqrt{6}\pi K_e}{l} \tag{1}$$

and the voltage generated by the motor e is given as

$$e = c_e \dot{d}_i \tag{2}$$

where d_i is the deformation of the rotational inertial mass, thus, $\dot{d}_i$ corresponds to the velocity of the motor part.

Moreover, let the current into the motor be i. Then the current i can be controlled using power electronics circuitry such as a MOSFET and governed based on the voltage e by

$$i(t) = -Y(t)e(t) \tag{3}$$

where $Y(t)$ is a feedback gain, which has units of admittance and the positive direction is determined so that the power defined as $i(t)e(t)$ becomes positive when energy flows the electrical circuit to the mechanical system. Note that, in this research, the single-directional converter is assumed for the current controllers, therefore the domain of $Y(t)$ is constrained by

$$Y(t) \in [0, Y^{\max}] \tag{4}$$

where $Y^{\max}$ is determined based on the performance of the power electronics circuitry and for an ideal system, $Y^{\max}$ must be less than or equal to the reciprocal of the internal or coil resistance of the motor R, i.e., $1/R$ (Cassidy and Scruggs 2013).

Next, let the displacement of the ET be d. For the case of the ET, the relationship expressed as $d_i = d$ must be satisfied. Thus, the force produced by the ET is derived as

$$f_t = m_i \ddot{d} + c_m \dot{d} - f_e \tag{5}$$

where the electromechanical force by the motor f_e is

$$f_e = c_e i \tag{6}$$

Also, the mechanical angle of the motor θ_m has a relationship with d_i; that is

$$\theta_m = \frac{2\pi}{l} d_i \tag{7}$$

Tuned inertial mass electromagnetic transducer

The TIMET proposed by the second author (Asai et al. 2017; Sugiura et al. 2020) is illustrated in Fig. 2 (a) schematically, which has an additional tuning spring and rotational mass producing larger inertance compared to the ET case introduced above. The simplified model of the TIMET can be represented as in Fig. 2 (b). In an analogous manner to the ET case, assume that d_i is the deformation of the rotational inertial mass part of the TIMET, then the force produced by the TIMET f_t can be expressed by Eq. (5) as well. Because the tuning spring is connected in series, f_t is equal to the forces by the tuning spring, so the equation expressed by

$$k_t(d - d_i) = f_t \tag{8}$$

is satisfied. Thus, we have the equation of motion given by

$$m_i \ddot{d}_i + c_m \dot{d}_i + k_t d_i = c_e i + k_t d \tag{9}$$

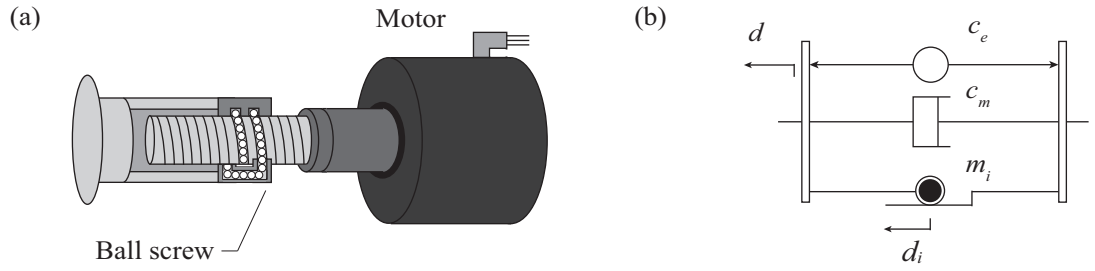

Figure 1. Electromagnetic transducer: (a) Schematic illustration, (b) Model.

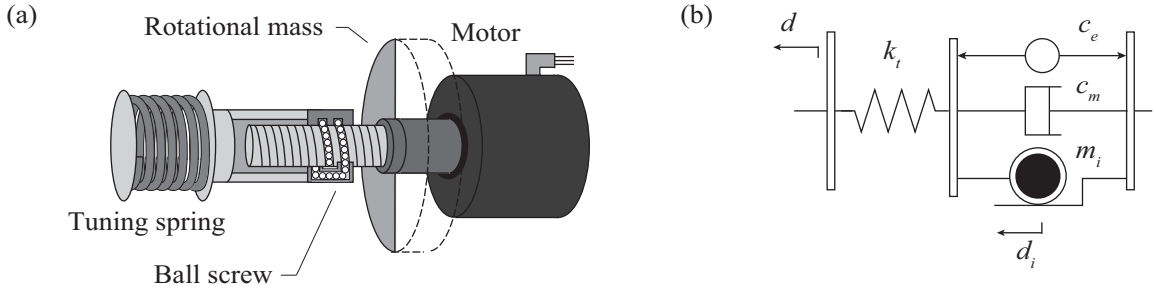

Figure 2. Tuned inertial mass lectromagnetic transducer: (a) Schematic illustration, (b) Model.

Therefore, from Eqs. (2) and (9), the state-space form for the system whose inputs are the motor current i and the displacement d and output is the voltage e is developed with the state $\mathbf{x}_h = \begin{bmatrix} d_i & \dot{d}_i \end{bmatrix}^T$ as

$$\dot{\mathbf{x}}_h(t) = \mathbf{A}_h \mathbf{x}_h(t) + \mathbf{B}_h i(t) + \mathbf{G}_h d(t) \tag{10}$$

$$e = \mathbf{C}_h \mathbf{x}_h \tag{11}$$

where

$$\mathbf{A}_h = \begin{bmatrix} 0 & 1 \\ -\frac{k_t}{m_i} & -\frac{c_m}{m_i} \end{bmatrix}, \quad \mathbf{B}_h = \begin{bmatrix} 0 \\ \frac{c_e}{m_i} \end{bmatrix}, \quad \mathbf{G}_h = \begin{bmatrix} 0 \\ \frac{k_t}{m_i} \end{bmatrix}, \quad \mathbf{C}_h = \begin{bmatrix} 0 & c_e \end{bmatrix} \tag{12}$$

Prototype of the proposed device

To change the inertance value m_i, the rotational mass part in Fig. 2 is redesigned. The photograph of the prototype fabricated for this research is depicted in Fig. 3. As shown in the figure, the prototype is attached to an actuator to apply excitation force and a load cell is placed between the prototype and the actuator to measure the reaction force.

In this section, the variable inerter mechanism of the prototype is described. Then, the parameter values of the prototype device are decided from the experimental data.

Variable mechanism

To realize the variable inerter mechanism simply by adding only one motor, the rotational mass part is redesigned as shown in Fig. 4 from the previous device (Sugiura et al. 2020; Asai et al. 2021). In the modified device, the rotational mass consists of six weights and an additional motor is installed in the prototype and the radius of rotation of the six weights r can be adjusted by changing the displacement d_v in Fig. 4 (b).

Let the moment of inertia be I, then the inertance m_i is defined with the lead of the ball screw l as

$$m_i = \left(\frac{2\pi}{l}\right)^2 I \tag{13}$$

Thus, m_i can be variable by changing the moment of inertia I. In the device, the moment of inertia I is given by the summation of the moment of inertias of the rotating weights around the ball screw I_w and other parts including the motor and axis I_o. The value of I_w is a function of the radius of rotation r, thus the inerter is also given as a function of r, that is

$$m_i(r) = \left(\frac{2\pi}{l}\right)^2 (I_w(r) + I_o) \tag{14}$$

From this equation, it is obvious that the inertance m_i can be adjusted by the additional motor.

Modeling

The parameters of the prototype are listed in Table 1. The motor employed for power generation here is a SGMJ-08A three-phase PMSM by YASKAWA and a precision ball screw manufactured by THK is used. The back EMF constant Ke is 0.584 Nm/Arms, which is provided in the specifications of the motor. Also, the internal or coil resistance R is 0.69Ω, which is measured with a LCR meter, and the effect of the coil inductance can be ignored here (Cassidy et al. 2011a). The lead of the ball screw l is 0.02 m and the stiffness of the tuning spring is 39240 N/m. It should be noted that the behavior of the three phase-motor is approximated by a single-phase DC motor for simplicity. For this conversion, the method with the Park transformation (Pillay and Krishnan 1989) introduced in (Cassidy et al. 2011a) is applied. Thus, the motor is treated as a single-DC motor for mathematical expressions in this article. For more details, refer to (Sugiura et al. 2020).

To confirm the change in inertance, three radius cases, i.e., minimum (r-min.), middle (r-mid.), and maximum (r-max.),

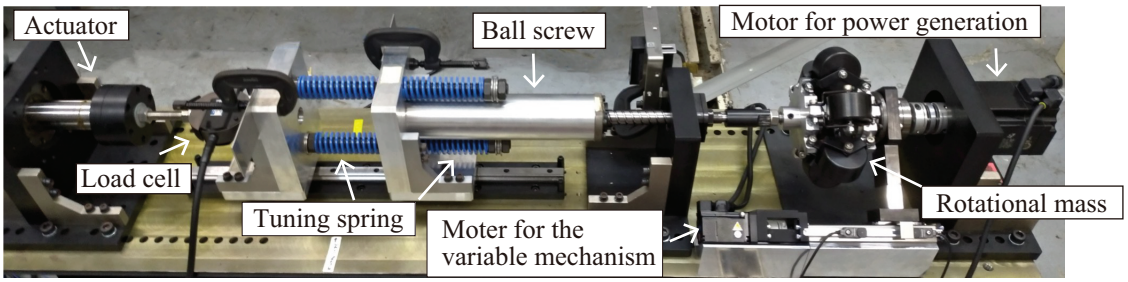

Figure 3. Prototype of the proposed device and experimental setup.

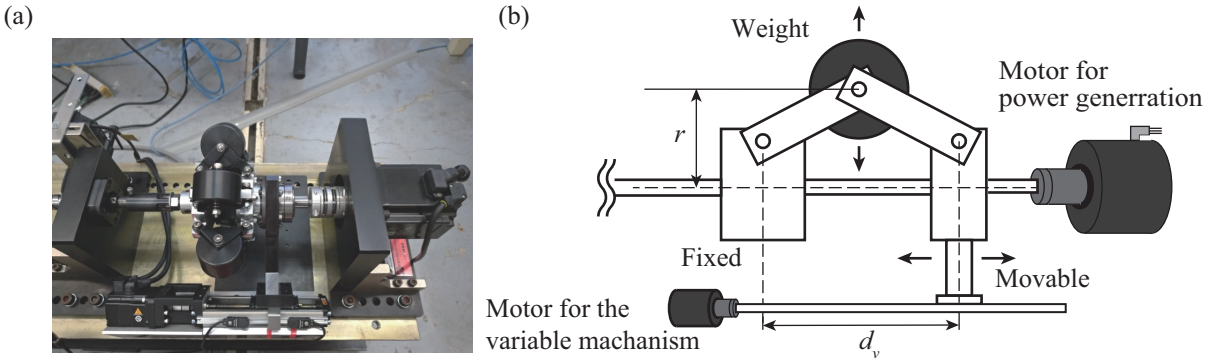

Figure 4. Variable mechanism: (a) Photograph, (b) Schematic illustration.

Table 1. Parameters

Parameter	r-min.	r-mid.	r-max.
K_e		0.584 Nm/Arms	
R		0.69 Ω	
l		0.02 m	
c_e		105.9 N/A	
k_t		39240 N/m	
m_i	1345.0 kg	1800.8 kg	2057.8 kg
c_m	1785.0 Ns/m	1945.5 Ns/m	2057.9 Ns/m

are investigated. It is difficult to estimate the exact values of the inertance m_i and the damping coefficient c_m for each case, so the prototype is connected to an actuator as shown in Fig. 3 and a sinusoidal sweep excitation with an amplitude 4 mm ranging from 0.5 to 1.0 Hz is input. Then, the inertance m_i and the damping coefficient c_m are determined from the experimental data by the curve fitting technique based on the least square method (Sugiura et al. 2020). The reaction force and the displacement of the inerter part of the experimental data and the estimated values obtained from the developed models for each case are compared in Fig. 5. As can be seen, the simulation results by the developed models show good agreement with the experimental data and the accuracy of the models is validated. The obtained values for the inertance and the damping coefficient are summarized in Table 1 as well, which shows that the inertance of the prototype can vary from 1345.0 kg to 2057.8 kg depending on the radius.

Problem formulation

Next, to design controllers to improve the power generation performance and apply them to the proposed device introduced in the previous sections, some formulations are carried out. In addition, the generated power is defined here.

Disturbance modeling

For many applications, the disturbance may be indefinite in the design phase. Thus, the stochastic control strategies are applied to the controller for the motor current i. As explained above, the prototype is attached to the actuator, thus the displacement of the prototype d is considered as the input disturbance in this paper. First, we assume that the disturbance displacement $d(t)$ is filtered white noise and its power spectral density equals to

$$S_d(\omega) = \left| \frac{jq\omega}{-\omega^2 + 2j\zeta_d\omega_d\omega + \omega_d^2} \right|^2 \tag{15}$$

where j is the imaginary unit (i.e., $j^2 = -1$), ω_d is the center of the passband of $d(t)$ and ζ_d determines the spread of its frequency content. For such a process, the disturbance dynamics is represented by a two-dimensional state-space of the form

$$\dot{\mathbf{x}}_d(t) = \mathbf{A}_d\mathbf{x}_d(t) + \mathbf{B}_d w(t) \tag{16}$$
$$d(t) = \mathbf{C}_d\mathbf{x}_d(t) \tag{17}$$

where

$$\mathbf{A}_d = \begin{bmatrix} 0 & 1 \\ -\omega_d^2 & -2\zeta_d\omega_d \end{bmatrix}, \quad \mathbf{B}_d = \begin{bmatrix} 0 \\ 2\sigma_d\sqrt{\zeta_d\omega_d} \end{bmatrix}, \quad \mathbf{C}_d = \begin{bmatrix} 0 & 1 \end{bmatrix} \tag{18}$$

and $w(t)$ is a white noise with spectral intensity equal to 1. The parameter q in Eq. (15) is adjusted such that $d(t)$ has a

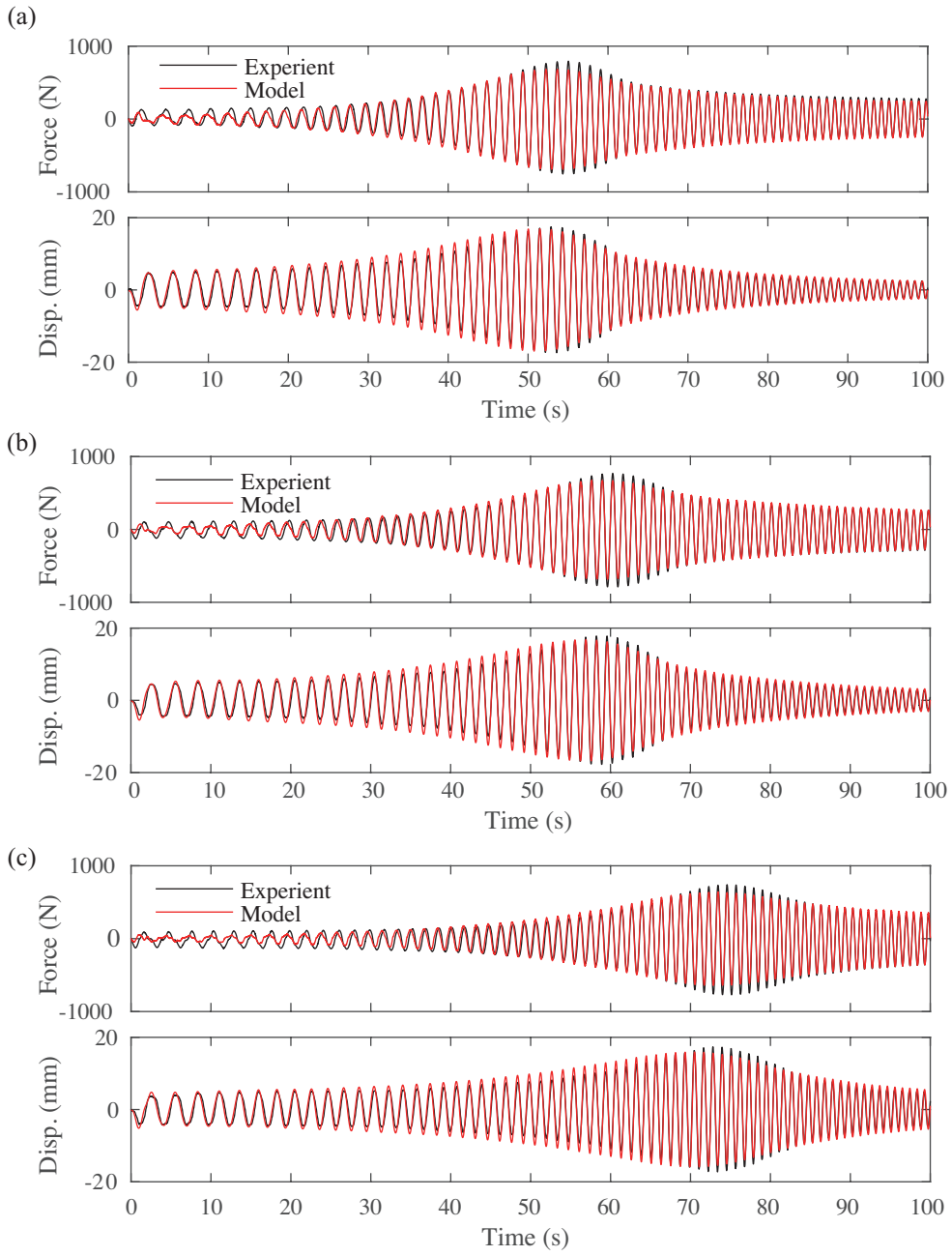

Figure 5. Comparisons of the reaction force and the displacement of the inerter part: (a) r-min., (b) r-mid., (c) r-max.

consistent standard deviation of σ_d, i.e.,

$$\sigma_d = \sqrt{\frac{1}{2\pi}\int_{-\infty}^{\infty} S_d(\omega)d\omega} \tag{19}$$

This allows us to compare energy harvesting performances from disturbances of varying spectral content but equal intensity. Note that when ζ_d is close to 0, the disturbance becomes narrowband random vibration. On the other hand, when a large value is chosen for ζ_d, the disturbance includes broadband frequency contents.

Augmented system

Combining the two dynamical systems for the device expressed by Eqs. (10) and (11) and the disturbance by Eqs. (16) and (17) yields an augmented system whose control input is the current i and disturbance input is white noise w and output is the voltage e given by

$$\dot{\mathbf{x}}(t) = \mathbf{A}\mathbf{x}(t) + \mathbf{B}i(t) + \mathbf{G}w(t) \tag{20}$$
$$e(t) = \mathbf{C}\mathbf{x}(t) \tag{21}$$

where the matrices $\mathbf{x}$, $\mathbf{A}$, $\mathbf{B}$, $\mathbf{G}$, and $\mathbf{C}$ are defined as

$$\mathbf{x} = \begin{bmatrix}\mathbf{x}_h \\ \mathbf{x}_d\end{bmatrix}, \quad \mathbf{A} = \begin{bmatrix}\mathbf{A}_h & \mathbf{G}_h\mathbf{C}_d \\ \mathbf{0} & \mathbf{A}_d\end{bmatrix}, \quad \mathbf{B} = \begin{bmatrix}\mathbf{B}_h \\ \mathbf{0}\end{bmatrix}, \quad \mathbf{G} = \begin{bmatrix}\mathbf{0} \\ \mathbf{B}_d\end{bmatrix}, \quad \mathbf{C} = \begin{bmatrix}\mathbf{C}_h & \mathbf{0}\end{bmatrix} \tag{22}$$

Energy harvesting objective

The energy harvesting objective for the system given by Eqs. (20) and (21) is defined here. In this paper, the power delivered to storage is assumed to be the generated power P_g, which is defined as the power extracted by

the harvester minus the transmission losses in the motor and power electronics circuitry. Generally, the transmission dissipation is quite complicated, and it depends not only on the electronic hardware used to realize the controller but also on the manner in which this hardware is operated such as its switching frequency, bus voltage, and gate voltage. However, for simplicity, the assumption that the power dissipated in the electronics is resistive is made here as in (Cassidy and Scruggs 2013). Therefore the generated power is defined as

$$P_g(t) = -i(t)e(t) - Ri^2(t) \tag{23}$$

in the time domain.

Provided these assumptions, the energy harvesting objective can be defined as the expectation of Eq. (23), i.e.,

$$\bar{P}_g = -\mathcal{E}\left\{ \begin{bmatrix} \mathbf{x} \\ i \end{bmatrix}^T \begin{bmatrix} \mathbf{0} & \frac{1}{2}\mathbf{C}^T \\ \frac{1}{2}\mathbf{C} & R \end{bmatrix} \begin{bmatrix} \mathbf{x} \\ i \end{bmatrix} \right\} \tag{24}$$

where $\mathcal{E}\{\cdot\}$ represent the expectation of $\{\cdot\}$. The objective for the motor current control algorithms introduced in the next section is to increase the power generation expressed by Eq. (24).

Control law

The inerter and the motor current are controlled to improve the power generation performance. This section introduces the algorithms employed in this article.

Inerter control

To control the inerter of the TIMET according to the change of the disturbance, a system to detect the dominant frequency provided by the Fast Fourier transform (FFT) using the the measured displacement data is developed.

Assume that N sequence data of the input displacement

$$\mathbf{d}_n = \begin{bmatrix} d_0 & d_1 & \cdots & d_{N-1} \end{bmatrix} \tag{25}$$

which are sampled at a frequency rate F_s, are used for the Fast Fourier transform given by

$$D_k = \sum_{n=0}^{N-1} d_n \exp \frac{2\pi j k n}{N} \tag{26}$$

where $k = 0, 1, \ldots, N-1$. The dominant frequency $f_{\max}$ is determined by

$$f_{\max} = \frac{F_s k_{\max}}{N} \tag{27}$$

where $k_{\max}$ is the value of k for the largest absolute value of Eq. (26) for $k = 0, 1, \ldots, \frac{N}{2}$, i.e.,

$$k_{\max} = \underset{k=0,1,\ldots,N/2}{\operatorname{argmax}} \begin{bmatrix} |D_0| & |D_1| & \cdots & |D_{N/2}| \end{bmatrix} \tag{28}$$

In the proposed device, the displacement of the input is measured by a laser displacement sensor and the inerter is controlled online based on the dominant frequency given by Eq. (27).

Motor current control

For the motor current control, two algorithms, static admittance (SA) and performance guaranteed (PG) controllers, introduced in (Cassidy and Scruggs 2013), are applied here. It was already shown that these two controllers works well for the TIMET in the authors previous works (Asai et al. 2017, 2021). Thus, the combined use with the inerter control is examined.

Static admittance control For the SA control, the feedback gain $Y(t)$ in Eq. (3) is restricted to a constant value, i.e., $Y(t) = Y_c$. Thus, the optimal constant value which maximizes the generated power given by Eq. (24) is adopted for Y_c of the SA control. The method to search for such a value is reviewed here.

From Eq. (3), the input current to the motor is expressed as a function of the state variable $\mathbf{x}$, i.e.,

$$i(t) = -Y_c e(t) \tag{29}$$

Substituting Eq. (29) into Eq. (20) yields the closed-loop dynamics having the form

$$\dot{\mathbf{x}}(t) = (\mathbf{A} - Y_c\mathbf{B}\mathbf{C})\mathbf{x}(t) + \mathbf{G}w(t) \tag{30}$$

Let the average power by the SA control be $\bar{P}_g^{\mathrm{SA}}$. Then for any time-invariant Y_c satisfying Eq. (4), it is a standard result that the power generation objective can be written as (Dorato et al. 1995)

$$\bar{P}_g{}^{\mathrm{SA}} = -\mathbf{G}^T\mathbf{S}_{\mathrm{SA}}\mathbf{G} \tag{31}$$

where $\mathbf{S}_{\mathrm{SA}} = \mathbf{S}_{\mathrm{SA}}^T < 0$ is the solution to the Lyapunov equation

$$\begin{aligned}(\mathbf{A} - Y_c\mathbf{B}\mathbf{C})^T\mathbf{S}_{\mathrm{SA}} + \mathbf{S}_{\mathrm{SA}}(\mathbf{A} - Y_c\mathbf{B}\mathbf{C}) \\ + \mathbf{C}^T(-Y_c + Y_c^2 R)\mathbf{C} = \mathbf{0}\end{aligned} \tag{32}$$

As mentioned previously, $Y^{\max}$ must be less than or equal to $1/R$, so the last term on the left-hand side of Eq. (32) is negative-semidefinite for all Y_c. Thus, since $\mathbf{A} - Y_c\mathbf{B}\mathbf{C}$ is asymptotically stable, the definiteness of $\mathbf{S}_{\mathrm{SA}}$ is assured by Lyapunov's second theorem (Stengel 1986). Then, the optimal value for Y_c is chosen so that Eq. (31) is maximized.

Performance guaranteed control For comparison, the efficacy of time-varying gain $Y(t)$ for the proposed device is examined. To control $Y(t)$, the PG control algorithm introduced in the literature is applied here. This algorithm is operated with a single-directional converter and the admittance Y becomes a function of time varying within the range of Eq. (4) so that the generated average power $\bar{P}_g^{\mathrm{PG}}$ must be larger than $\bar{P}_g^{\mathrm{SA}}$, i.e.,

$$\bar{P}_g^{\mathrm{PG}} \geq \bar{P}_g^{\mathrm{SA}} \tag{33}$$

In the PG control algorithm, the admittance is controlled by

$$Y(t) = \underset{[0, Y^{\max}]}{\mathrm{sat}}\left\{ \frac{\mathbf{K}\mathbf{x}}{e} \right\} \tag{34}$$

where

$$\mathbf{K} = -\frac{1}{R}\left(\mathbf{B}^T\mathbf{S}_{\mathrm{SA}} + \frac{1}{2}\mathbf{C} \right) \tag{35}$$

Note that Y_c is the constant value for the SA control. In this case, the current i is expressed by

$$i(t) = \begin{cases} i_u(t) & : i_u e + i_u^2/Y^{\max} \leq 0 \\ 0 & : i_u e + i_u^2/Y^{\max} > 0 \text{ and } i_u e > 0 \\ -Y^{\max} e(t) & : \text{otherwise} \end{cases} \tag{36}$$

where

$$i_u(t) = -\mathbf{K}\mathbf{x} \tag{37}$$

Kalman filter

To implement the PG control introduced above, the full state $\mathbf{x}$ needs to be measured. However, it is not practical to measure all the state values in $\mathbf{x}$. Therefore the estimated state $\hat{\mathbf{x}}$ obtained by the Kalman filter (Kalman 1960; Kalman and Bucy 1961) is used instead of $\mathbf{x}$ for the PG control.

For the Kalman filter design, we assume that the motor voltage e and the input displacement d, which is used for the inerter control, are measurable. Define the measurable output as

$$\mathbf{y}_m = \begin{bmatrix} e \\ d \end{bmatrix} = \mathbf{C}_m \mathbf{x} \tag{38}$$

then the state-space equation of the Kalman filter is given by

$$\dot{\hat{\mathbf{x}}} = (\mathbf{A} - \mathbf{L}\mathbf{C}_m)\hat{\mathbf{x}} + \mathbf{B}i + \mathbf{L}\mathbf{y}_m \tag{39}$$

where $\mathbf{L}$ is the Kalman gain, which is defined as

$$\mathbf{L} = \mathbf{P}_e \mathbf{C}_m^T \mathbf{V}_n^{-1} \tag{40}$$

and $\mathbf{P}_e = \mathbf{P}_e^T$ is the solution of the algebraic Ricatti equation given by

$$\mathbf{A}\mathbf{P}_e + \mathbf{P}_e\mathbf{A}^T - \mathbf{P}_e\mathbf{C}_m\mathbf{V}_n^{-1}\mathbf{C}_m\mathbf{P}_e - \mathbf{G}W_n\mathbf{G}^T = \mathbf{0} \tag{41}$$

where W_n and $\mathbf{V}_n$ are magnitude of the constant power spectral densities for the white noises. As stated before, $\hat{\mathbf{x}}$ is used instead of $\mathbf{x}$ for the PG control given by Eqs. (34) and (36).

Experimental verification

The effectiveness of the proposed energy harvester with the variable inerter mechanism controlled by the algorithms introduced above is shown through dynamic testing. Then, the results are compered with the numerical simulation results to examine the validity of the developed models.

Experimental setup

The experimental setup of the prototype device is shown in Fig. 3. A dSPACE MicroLabBox is utilized to implement the controllers and acquire data here.

For validation of the variable tuned inerter mechanism, a sinusoidal sweep wave and a random wave are used as input displacements of the actuator. The time histories of these two inputs are shown in Fig. 6. The frequency of the sinusoidal sweep wave varies from 0.5 Hz to 1.0 Hz gradually for 200 s. While the random wave is generated from a white noise from Eqs. (16), (17), and (18). For the random wave, the dominant frequency property is changed in the middle of excitation as follows; $\omega_a = 5.03$, $\zeta_a = 0.1$, and $\sigma_a = 0.0025$ for the first 100 s and $\omega_a = 4.08$, $\zeta_a = 0.1$, and $\sigma_a = 0.0025$ for the last 100 s.

Table 2. Average power to the sinusoidal sweep wave input.

	SA (W)		PG (W)	
	Exp.	Sim.	Exp.	Sim.
r-min.	1.983	1.901	2.309	2.101
r-mid.	2.279	2.001	2.652	2.345
r-max.	2.571	2.201	2.700	2.325
r-variable	3.464	2.665	3.508	2.838

To design the inerter controller, the power generation performances of the three constant inerter cases are simulated beforehand using the developed models given in Table 1. The results to a sinusoidal sine wave ranging from 0.5 Hz to 1 Hz with an amplitude of 5 mm are compared in Fig. 7. As can be observed, the r-min. case shows the best energy harvesting performance for the input of less than 0.696 Hz, the r-mid. case for the input between 0.696 Hz and 0.780 Hz, and the r-max. case for the input of more than 0.780 Hz. Thus, in this experiment, the inertance is controlled discretely to be at the three positions of r-min., r-mid. and r-max. according to the measured dominant frequency to maximize the power generation capability and the variable inerter case is referred to r-variable. The parameters to carry out the FFT for the r-variable case are set to $N = 2048$ and $F_s = 150$ Hz in Eq. (27). Also, 50% of the measured data or 1024 data points are allowed to be overlapped to implement the FFT so that the update frequency is increased. Thus, the frequency resolution becomes $\frac{F_s}{N} = 0.0732$ Hz and the update period of the dominant frequency is $\frac{N}{2F_s} = 6.8267$ s. These parameters are decided so that the prototype works effectively considering the effective frequency range of the prototype shown in Fig. 7. For comparison, in addition to the r-variable case, the three constant inerter cases are investigated as well.

The two motor current controllers are designed individually, depending on the inertance value, because the parameters required for the controller design are different for each case. Thus, for the r-variable case, the parameters for the motor current controller are modified along with the inertance change during excitation. The domain of of admittance is restricted conservatively by $Y^{\max} = 0.694$ Ω^{-1} which satisfies the condition of $Y^{\max} < \frac{1}{R}$. For the Kalman filter, the displacement input data measured by the laser displacement sensor, which is the same data for the inerter controller, is used. Also, the voltage date can be measured by the MicroLabBox.

Results

The average power for 200 s excitation obtained from experiments are summarized in Tables 2 and 3, which demonstrate the effectiveness of the proposed variable inerter mechanism in vibration energy harvesting. In particular, the results show that the combination of the inerter control and the PG control works very well to both sinusoidal sine and random waves.

The time histories of the power generation to the sinusoidal sweep wave are shown in Figs. 8 and 9. As can be observed, the variable inerter mechanism works well to improve the power generation in the wide frequency range

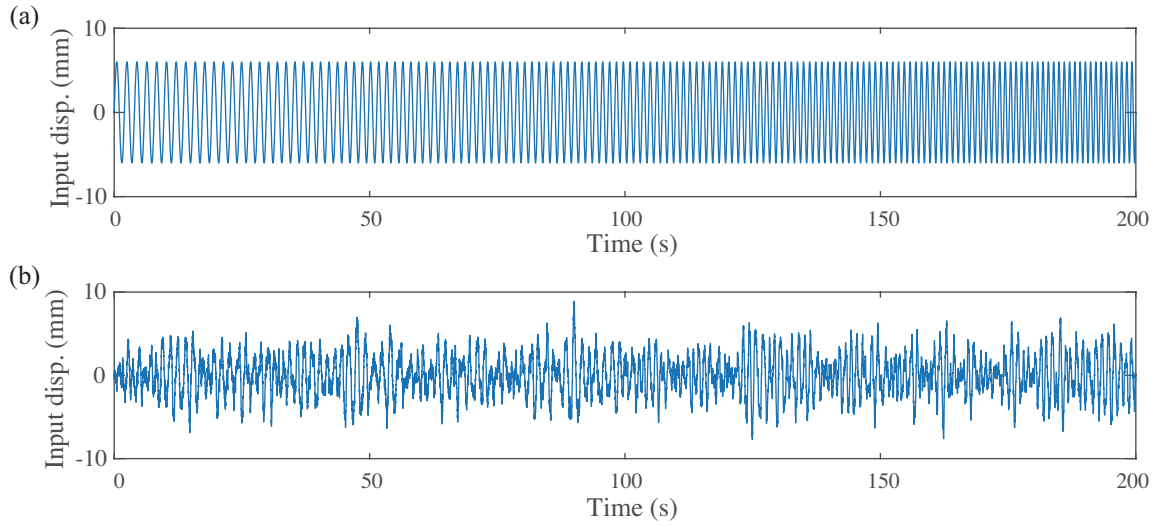

Figure 6. Input displacement: (a) Sinusoidal sweep wave, (b) Random wave.

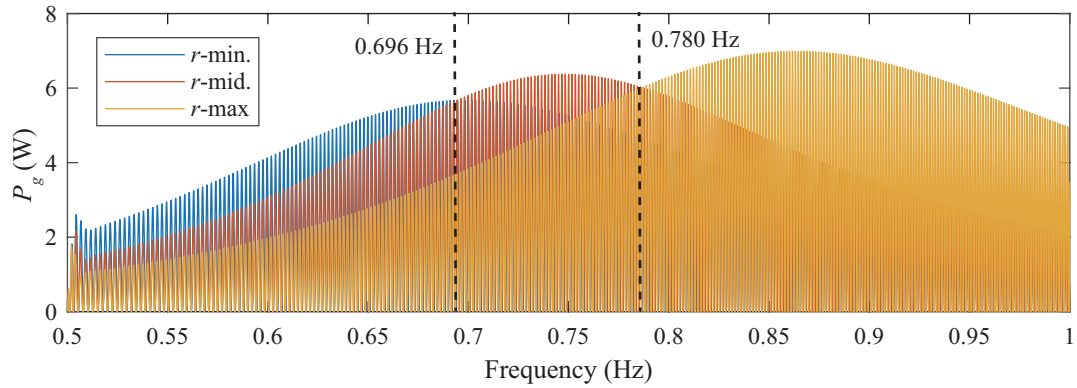

Figure 7. Comparison of the power generation performances of the three constant inerter cases.

Table 3. Average power to the random wave input.

	SA (W)		PG (W)	
	Exp.	Sim.	Exp.	Sim.
r-min.	0.435	0.586	0.493	0.623
r-mid.	0.440	0.619	0.500	0.693
r-max.	0.432	0.646	0.487	0.707
r-variable	0.499	0.687	0.567	0.714

and shows the superiority of the proposed device over the constant inerter cases for both SA and PG controllers.

The random wave cases are shown in Figs. 10 and 11 as well. It is difficult to tell the difference in these figures, however, we can see a slight improvement in power generation of the variable inerter case over the three constant cases.

The time histories of the dominant frequency detected from the method introduced in the previous section are shown in Fig. 12. For the sinusoidal sweep wave, the calculated dominant frequency increases gradually along the change of the input frequency. And for the random wave, the dominant frequency goes back and force in the range of 0.780 Hz or less for most of the first 100 s and varies within a range of not less than 0.696 Hz for the last 100 s. While, for both input waves, the detected dominant frequencies until the first $N = 2048$ data are collected does not make any sense because these values are calculated by the noise data before the excitation starts. Furthermore, the dominant frequency calculated by the FFT are based on the past data, thus, the obtained value does not necessarily indicate the current dominant frequency, that is, there is an unavoidable time lag in this strategy. Overall, it is shown that the developed system can detect the dominant frequency relatively accurately online and improve the power generation performance; however, the time lag caused by the FFT is the issue to be addressed.

A part of the time histories of admittance for r-variable case are plotted in Figs. 13 and 14. It is confirmed that the admittance value is constant depending on the inertance for the SA control. While, when the PG control is applied to both sinusoidal sweep and random wave inputs, it is observed that the admittance is controlled smoothly by the algorithm defined by Eq. (34).

Comparisons with numerical simulation

Finally, the average power calculated from the numerical simulations using the parameter given in Table are summarized in Tables 2 and 3 as well. In these tables, some discrepancies between the experiments and the simulations can be found especially when the inertance value is variable or the random wave is input. We can assume that these discrepancies are attributable to the modeling errors mainly

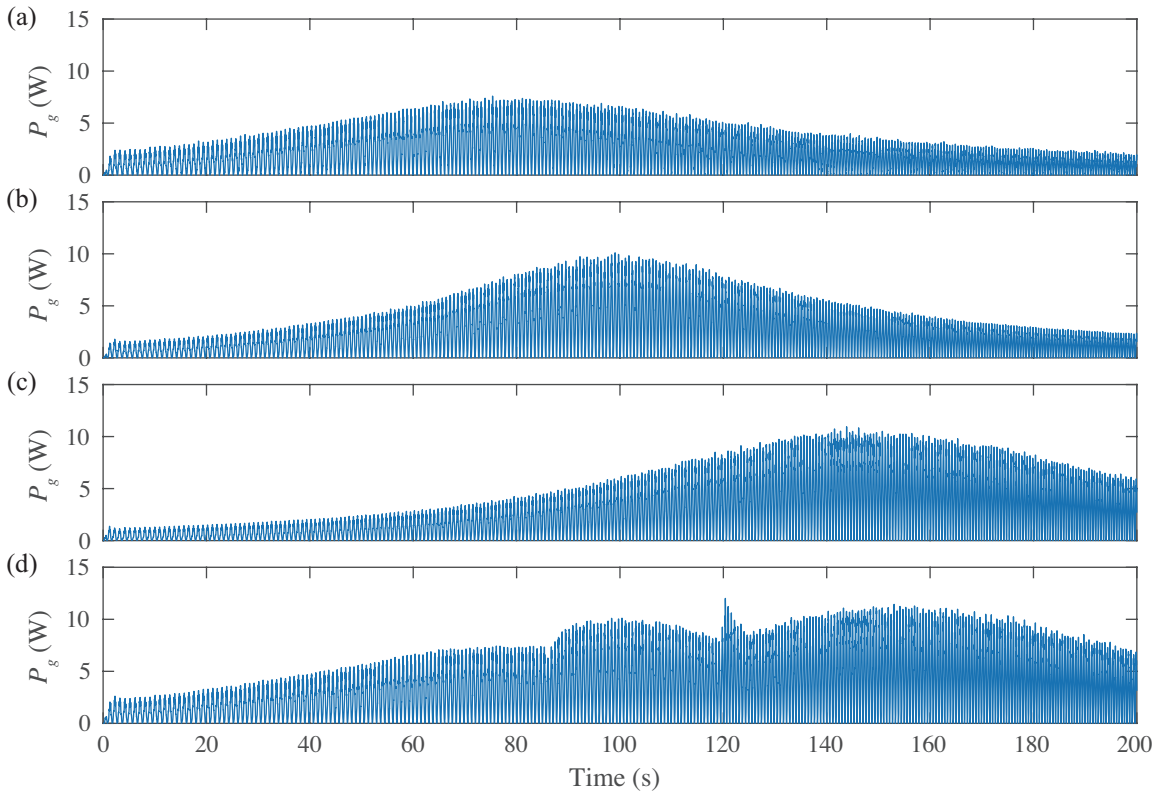

Figure 8. Power generation for SA control to sinusoidal sweep wave: (a) r-min., (b) r-mid., (c) r-max., (d) r-variable.

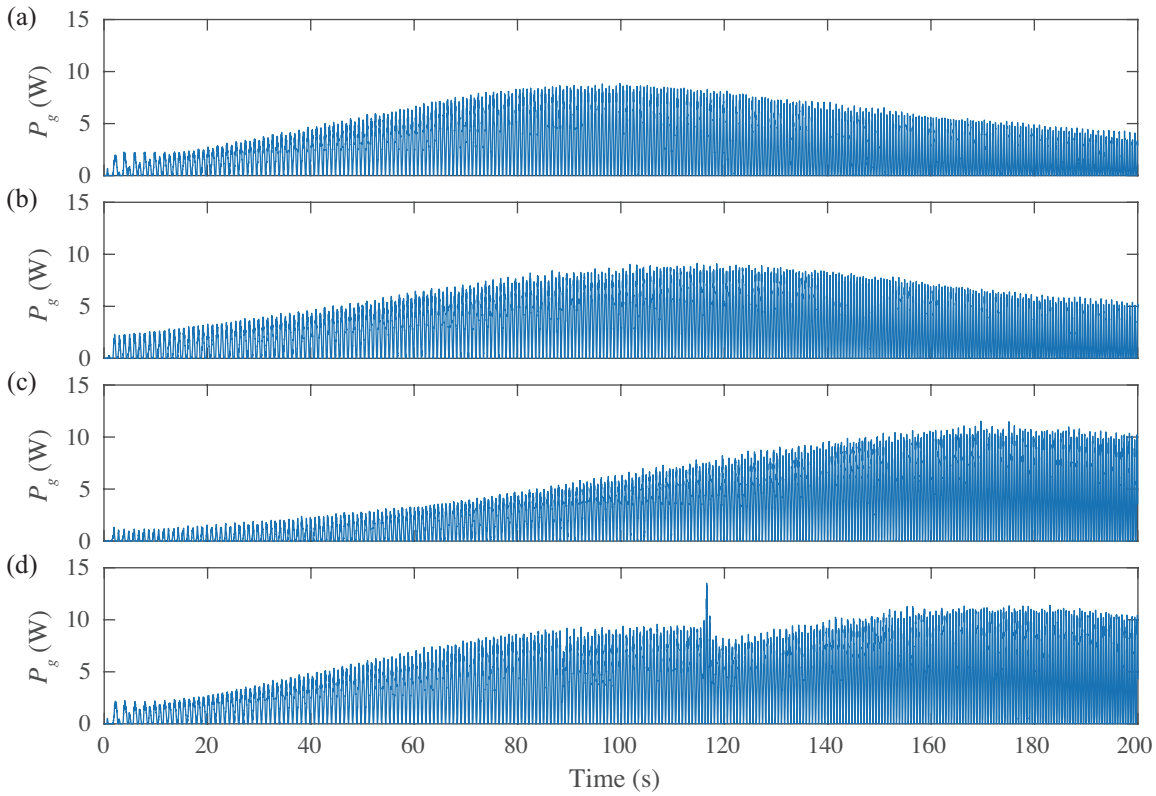

Figure 9. Power generation for PG control to sinusoidal sweep wave: (a) r-min., (b) r-mid., (c) r-max., (d) r-variable.

in the damping part. As stated previously, the damping element of the device is modeled as a liner damping for simplicity here based on the least square method using the sinusoidal sweep excitation for each constant radius value. Thus, the simulation results for the fixed inertance cases to the sinusoidal sweep wave agrees relatively well with the experimental results, while non-negligible errors are observed in other cases and these errors might be improved by developing nonlinear models considering various factors such as friction. However, the numerical results obtained

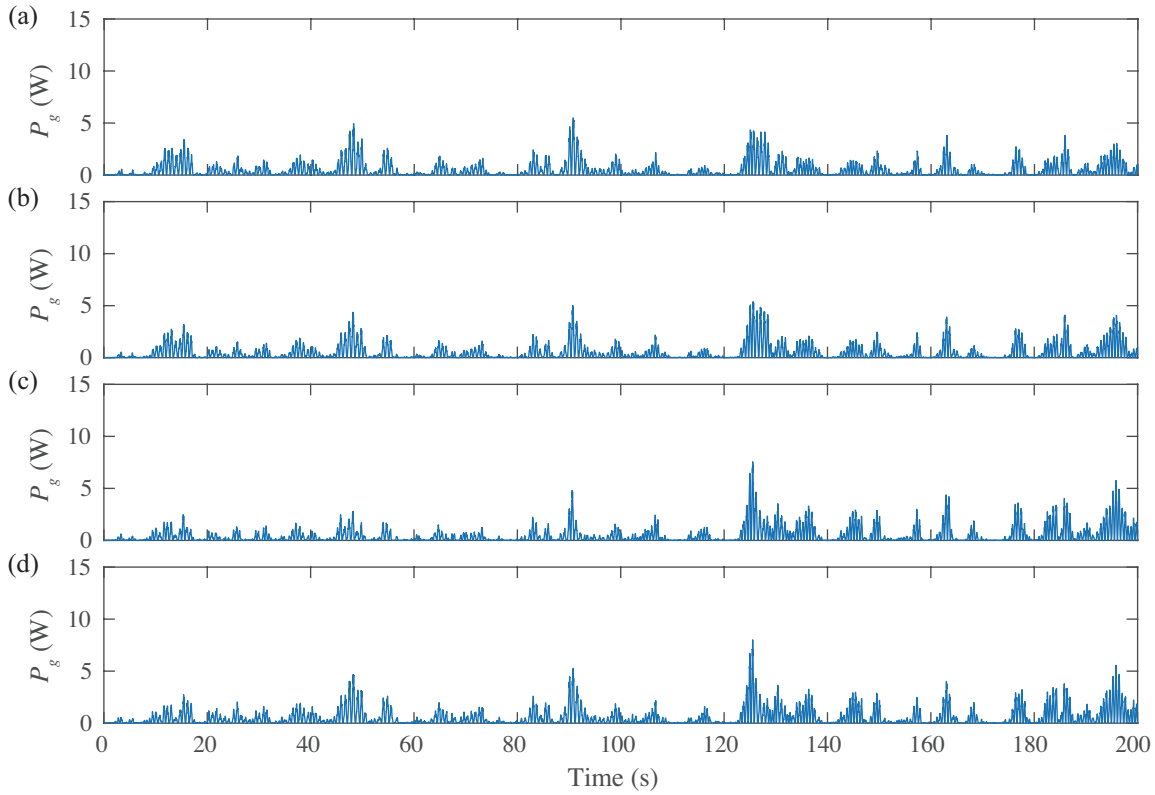

Figure 10. Power generation for SA control to random wave: (a) r-min., (b) r-mid., (c) r-max., (d) r-variable.

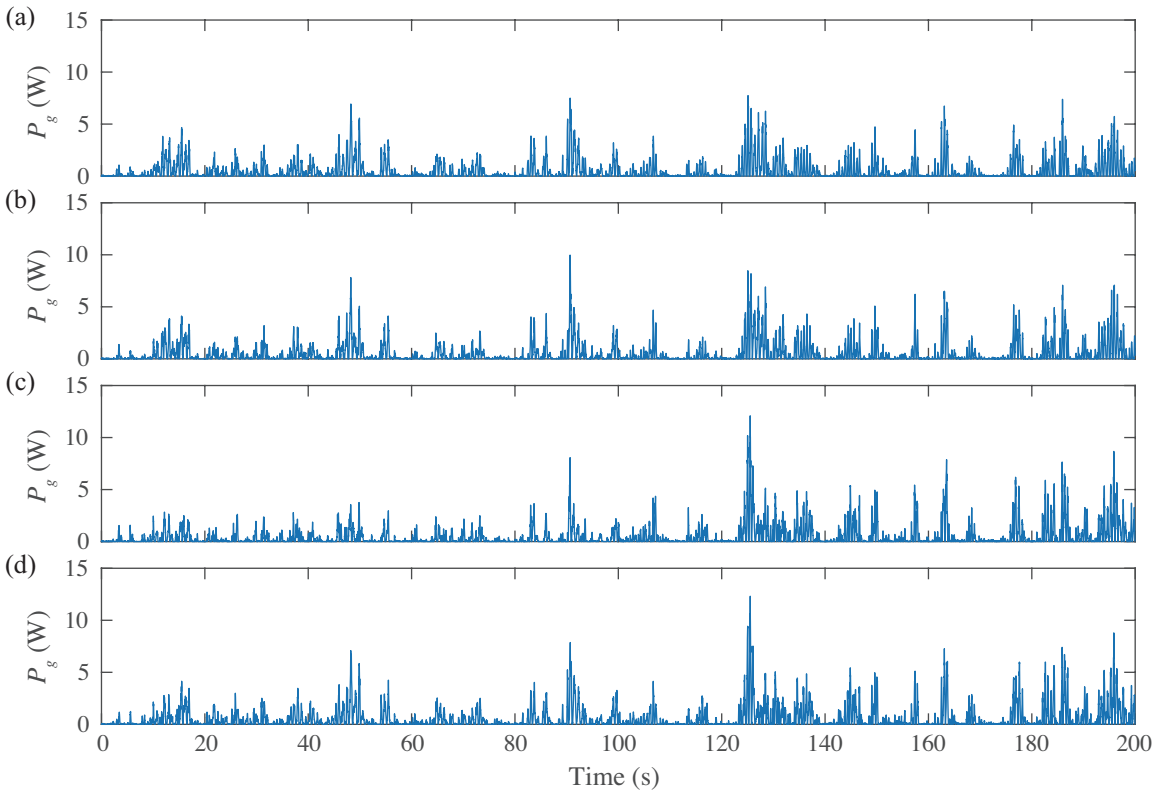

Figure 11. Power generation for PG control to random wave: (a) r-min., (b) r-mid., (c) r-max., (d) r-variable.

here also show the validity of the variable inerter mechanism for the TIMET.

Conclusions

This paper presented a novel vibration energy harvesting device employing a tuned variable inerter and introduced the system to control the inertance value based on the dominant

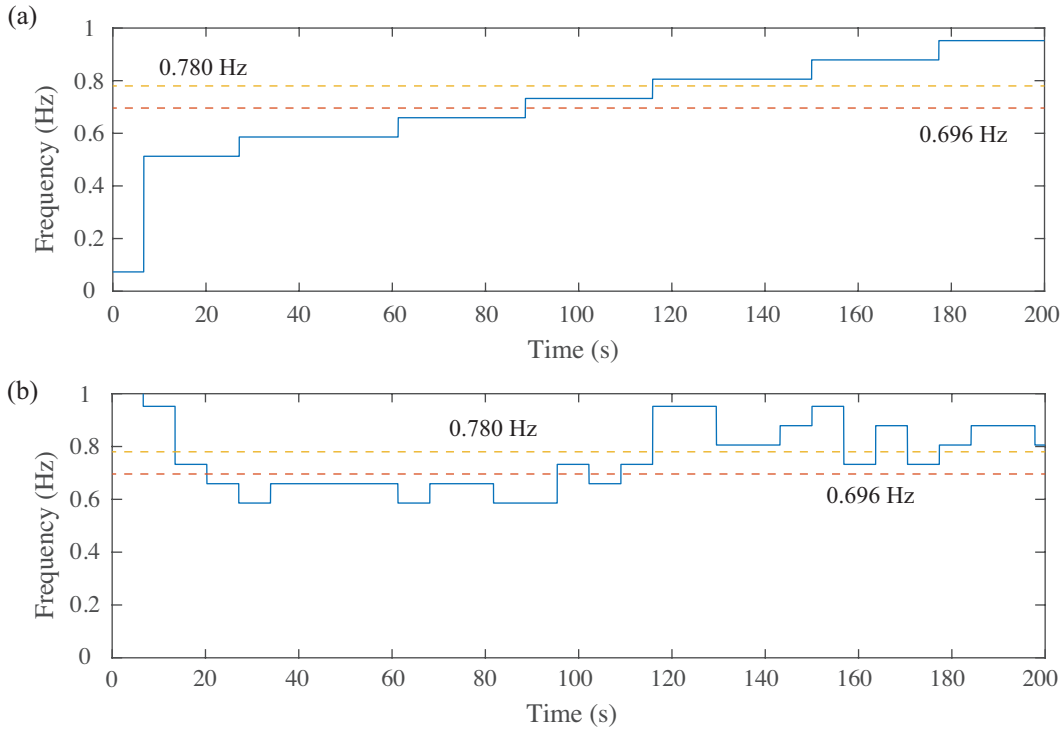

Figure 12. Dominant frequency detected during excitation tests: (a) Sinusoidal sweep wave, (b) Random wave.

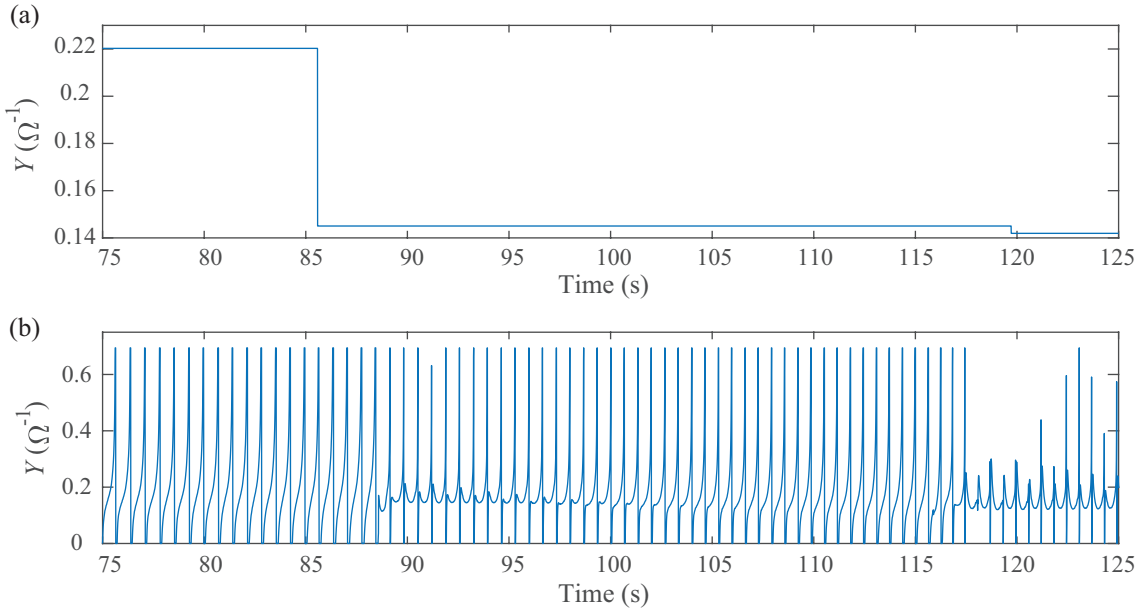

Figure 13. Admittance to sinusoidal sweep wave for r-variable case: (a) SA control, (b) PG control.

frequency detected by the measured data through the FFT technique. A prototype of the proposed device was fabricated and it was shown through excitation tests that the energy harvesting performance of the TIMET can be increased by adjusting the inerter value along with the appropriate motor current control.

However, the FFT uses the past data, thus, the dominant frequency provided by the FFT has a time lag from the actual state. Therefore, the proposed strategy is unsuitable for the systems subject to rapidly changing disturbances. Also, controlling the inertance value requires additional energy, which was not considered in this article. To address these issues, other control algorithms for the variable inerter mechanism should be investigated. In particular, model predictive control (MPC) is considered to be promising because the optimum controller is redesigned at every time step in the MPC strategy. Moreover, it is necessary to carefully consider the applications and design methods that can maximize the advantage of the present device considering the energy the required for the variable inerter mechanism. In addition, developing more accurate models considering the nonlinearity of the device to evaluate energy loss more precisely and implementing experiments with a larger size prototype are necessary as well for future work.

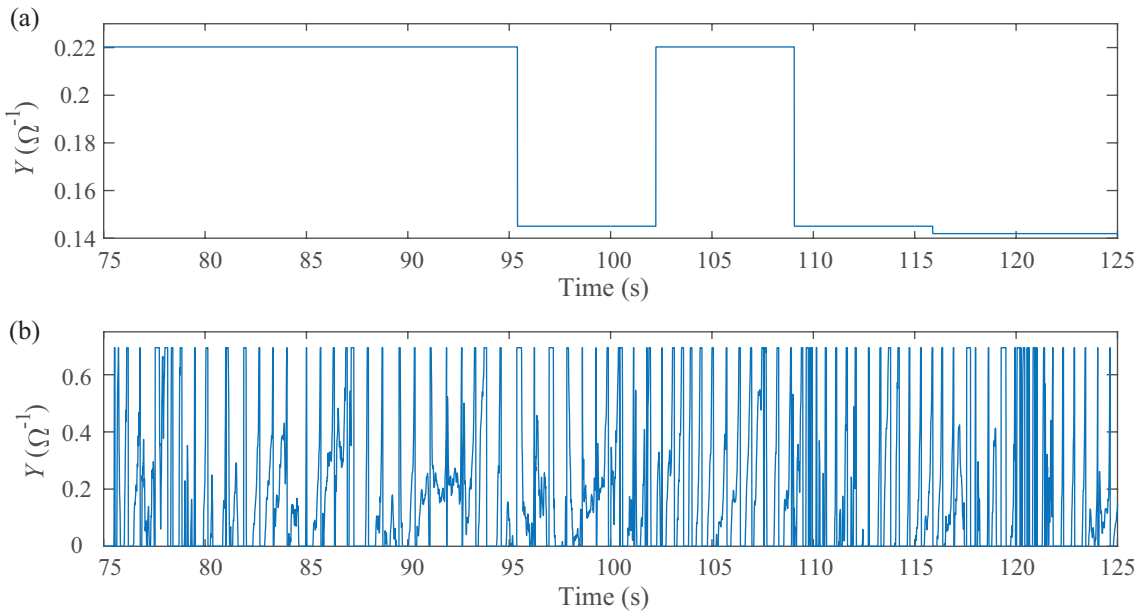

Figure 14. Admittance to random wave for r-variable case: (a) SA control, (b) PG control.

Acknowledgements

This work was supported financially by JSPS KAKENHI Grant number 17H04942 which is gratefully appreciated.

References

Asai T, Araki Y and Ikago K (2017) Energy harvesting potential of tuned inertial mass electromagnetic transducers. *Mechanical Systems and Signal Processing* 84, Part A: 659 – 672. DOI: 10.1016/j.ymssp.2016.07.048.

Asai T and Scruggs JT (2016) Nonlinear stochastic control of self-powered variable-damping vibration control systems. In: *2016 American Control Conference (ACC)*. pp. 442–448. DOI: 10.1109/ACC.2016.7524954.

Asai T, Takino M, Watanabe Y and Sugiura K (2021) Hardware-in-the-loop testing of an electromagnetic transducer with a tuned inerter for vibratory energy harvesting. *ASCE-ASME Journal of Risk and Uncertainty in Engineering Systems, Part B: Mechanical Engineering* 7(1): 010908. DOI:10.1115/1.4049231.

Caruso G, Galeani S and Menini L (2018) Semi-active damping and energy harvesting using an electromagnetic transducer. *Journal of Vibration and Control* 24(12): 2542–2561. DOI: 10.1177/1077546316688993.

Cassidy I, Scruggs J, Behrens S and Gavin HP (2011a) Design and experimental characterization of an electromagnetic transducer for large-scale vibratory energy harvesting applications. *Journal of Intelligent Material Systems and Structures* 22(17): 2009–2024. DOI:10.1177/1045389X11421824.

Cassidy IL and Scruggs JT (2013) Nonlinear stochastic controllers for power-flow-constrained vibratory energy harvesters. *Journal of Sound and Vibration* 332(13): 3134 – 3147.

Cassidy IL, Scruggs JT and Behrens S (2011b) Optimization of partial-state feedback for vibratory energy harvesters subjected to broadband stochastic disturbances. *Smart Materials and Structures* 20(8): 085019. DOI:10.1088/0964-1726/20/8/085019.

Dorato P, Abdallah C and Cerone V (1995) *Linear Quadratic Control: An Introduction*. Krieger Publishing Company. ISBN 9781575241562.

Faraj R, Jankowski U, Graczykowski C and Holnicki-Szulc J (2019) Can the inerter be a successful shock-absorber? the case of a ball-screw inerter with a variable thread lead. *Journal of the Franklin Institute* 356(14): 7855–7872. DOI:https://doi.org/10.1016/j.jfranklin.2019.04.012. Special Issue on Inerter-based Systems.

Gonzalez-Buelga A, Clare LR, Neild SA, Jiang JZ and Inman DJ (2015) An electromagnetic inerter-based vibration suppression device. *Smart Materials and Structures* 24(5): 055015.

Ikago K, Saito K and Inoue N (2012) Seismic control of single-degree-of-freedom structure using tuned viscous mass damper. *Earthquake Engineering & Structural Dynamics* 41(3): 453–474. DOI:10.1002/eqe.1138.

Jamshidi M, Chang C and Bakhshi A (2017) Self-powered hybrid electromagnetic damper for cable vibration mitigation. *Smart Structures Systems* 20(3): 285–301. DOI:10.12989/sss.2017.20.3.285.

Kalman RE (1960) A new approach to linear filtering and prediction problems. *ASME Journal of Basic Engineering* .

Kalman RE and Bucy RS (1961) New results in linear filtering and prediction theory. *TRANS. ASME, SER. D, J. BASIC ENG* : 109.

Lazar IF, Neild S and Wagg D (2014) Using an inerter-based device for structural vibration suppression. *Earthquake Engineering & Structural Dynamics* 43(8): 1129–1147. DOI:10.1002/eqe.2390.

Lazarek M, Brzeski P and Perlikowski P (2019) Design and modeling of the cvt for adjustable inerter. *Journal of the Franklin Institute* 356(14): 7611–7625. DOI:https://doi.org/10.1016/j.jfranklin.2018.11.011. Special Issue on Inerter-based Systems.

Ma R, Bi K and Hao H (2021) Inerter-based structural vibration control: A state-of-the-art review. *Engineering Structures* 243: 112655. DOI:https://doi.org/10.1016/j.engstruct.2021.112655.

Marian L and Giaralis A (2014) Optimal design of a novel tuned mass-damper-inerter (tmdi) passive vibration control configuration for stochastically support-excited structural systems. *Probabilistic Engineering Mechanics* 38: 156 – 164. DOI:https://doi.org/10.1016/j.probengmech.2014.03.007.

Marian L and Giaralis A (2017) The tuned mass-damper-inerter for harmonic vibrations suppression, attached mass reduction, and energy harvesting. *Smart structures and systems* 19(6): 665–678. DOI:10.12989/sss.2017.19.6.665.

Monaco FD, Tehrani MG, Elliott SJ, Bonisoli E and Tornincasa S (2013) Energy harvesting using semi-active control. *Journal of Sound and Vibration* 332(23): 6033 – 6043. DOI:https://doi.org/10.1016/j.jsv.2013.06.005.

Nakano K, Suda Y and Nakadai S (2003) Self-powered active vibration control using a single electric actuator. *Journal of Sound and Vibration* 260(2): 213 – 235. DOI:https://doi.org/10.1016/S0022-460X(02)00980-X.

Pillay P and Krishnan R (1989) Modeling, simulation, and analysis of permanent-magnet motor drives. i. the permanent-magnet synchronous motor drive. *IEEE Transactions on Industry Applications* 25(2): 265–273. DOI:10.1109/28.25541.

Scruggs JT and Iwan WD (2003) Control of a civil structure using an electric machine with semiactive capability. *Journal of Structural Engineering* 129(7): 951–959. DOI:10.1061/(ASCE)0733-9445(2003)129:7(951).

Shen W, Zhu S and Zhu H (2019) Unify energy harvesting and vibration control functions in randomly excited structures with electromagnetic devices. *Journal of Engineering Mechanics* 145(1): 04018115. DOI:10.1061/(ASCE)EM.1943-7889.0001548.

Siang J, Lim M and Salman Leong M (2018) Review of vibration-based energy harvesting technology: Mechanism and architectural approach. *International Journal of Energy Research* 42(5): 1866–1893. DOI:10.1002/er.3986.

Smith MC (2002) Synthesis of mechanical networks: the inerter. *IEEE Transactions on Automatic Control* 47(10): 1648–1662. DOI:10.1109/TAC.2002.803532.

Stengel R (1986) *Optimal Control and Estimation*. Dover books on advanced mathematics. Dover Publications. ISBN 9780486682006.

Sugiura K, Watanabe Y, Asai T, Araki Y and Ikago K (2020) Experimental characterization and performance improvement evaluation of an electromagnetic transducer utilizing a tuned inerter. *Journal of Vibration and Control* 26(1-2): 56–72. DOI:10.1177/1077546319876396.

Wagg DJ (2021) A review of the mechanical inerter: historical context, physical realisations and nonlinear applications. *Nonlinear Dynamics* 104(1): 13–34. DOI:10.1007/s11071-021-06303-8.

Wei C and Jing X (2017) A comprehensive review on vibration energy harvesting: Modelling and realization. *Renewable and Sustainable Energy Reviews* 74: 1 – 18. DOI:https://doi.org/10.1016/j.rser.2017.01.073.

Zhu H, Li Y, Shen W and Zhu S (2019) Mechanical and energy-harvesting model for electromagnetic inertial mass dampers. *Mechanical Systems and Signal Processing* 120: 203 – 220. DOI:https://doi.org/10.1016/j.ymssp.2018.10.023.

Zuo L and Tang X (2013) Large-scale vibration energy harvesting. *Journal of Intelligent Material Systems and Structures* 24(11): 1405–1430. DOI:10.1177/1045389X13486707.